Deep Learning Aided Fingerprint Based Beam Alignment for mmWave Vehicular Communication

K. Satyanarayana, *Student Member, IEEE*, Mohammed El-Hajjar, *Senior Member, IEEE*, Alain Mourad, Lajos Hanzo, *Fellow, IEEE*

***Abstract*—Harnessing the substantial bandwidth available at millimeter wave (mmWave) carrier frequencies has proved to be beneficial to accommodate a large number of users with increased data rates. However, owing to the high propagation losses observed at mmWave frequencies, directional transmission has to be employed. This necessitates efficient beam-alignment for a successful transmission. Achieving perfect beam-alignment is however challenging, especially in the scenarios when there is a rapid movement of vehicles associated with ever-changing traffic density, which is governed by the topology of roads as well as the time of the day. Therefore, in this paper, we take the approach of fingerprint based beam-alignment, where a set of beam pairs constitute the fingerprint of a given location. Furthermore, given the time-varying traffic density, we propose a multi-fingerprint based database for a given location, where the base station (BS) intelligently adapts the fingerprints with the aid of learning. Additionally, we propose multi-functional beam transmission as an application of our proposed design, where the beam-pairs that satisfy the required received signal strength (RSS) participate in increasing the spectral efficiency or improving the end-to-end performance in some other way. Explicitly, the BS leverages the plurality of beam-pairs to attain both multiplexing and diversity gains. Furthermore, if the plurality of beam-pairs is higher than the number of RF chains, the BS may also employ beam-index modulation to further improve the spectral efficiency. We demonstrate that having multiple fingerprint-based beam-alignment provides superior performance than that of the single fingerprint based beam-alignment. Furthermore, we show that our learning-aided multiple fingerprint design provides a better fidelity compared to that of the benchmark scheme also employing multiple fingerprint but dispensing with learning. Additionally, our reduced-search based learning-aided beam-alignment design performs similarly to beam-sweeping based beam-alignment, even though an exhaustive beam-search is carried out by the latter. More explicitly, our design is capable of maintaining the target performance in dense vehicular environments, while both single fingerprint and line-of-sight (LOS) based beam-alignment suffer from blockages.**

***Index Terms*—Millimeter Wave, MIMO, Beamforming, Machine Learning.**

I. Introduction

GIVEN the rapid proliferation of wireless devices and the increase in the data rate demands of the mobile phone users, harnessing mmWave frequencies owing to its large bandwidth constitutes a promising solution for next-generation wireless communications [1]. However, one of the key challenges upon using mmWave frequencies is that they suffer from high propagation losses because of the attenuation due to atmospheric absorption, foliage density and rain-induced fading [1]. To mitigate these effects directional transmission has to be employed, where the signal is steered in the direction of the user. To achieve this, a large antenna array can be mounted on both the BS and mobile station [2], where narrow beams emanate from the transmit beamforming array. Because of the narrow beams and high susceptibility of mmWave frequencies to blockages, aligning the beams of departure and arrival is challenging. The probability of beam misalignment is even higher when the environment is continuously changing as in vehicular environments [3], [4], which maybe attributed to the ever-changing traffic because of the time-varying movement of vehicles. The mobility of vehicles is different at different times of the day [5]. Furthermore, the traffic density is dependent on the topology of roads [5]. Thus, by considering all the parameters such as spatial randomness and vehicular speeds, it was found that the number of vehicles at any time obeys Poisson distribution with a mean of λ [5], [6]. Therefore, in this treatise, we model the traffic density by a Poisson process.

Establishing perfect beam-alignment would necessitate the knowledge of both the angle-of-arrival (AoA) and the angle-of-departure (AoD). The AoA/AoD may be determined as part of channel estimation; however, to perform channel estimation prior to beam-alignment fails to exploit the beamforming gain, which is vital for reliable communication over mmWave links. Hence to circumvent this problem, conventionally beam-alignment is carried out using exhaustive beam sweeping, where the BS and the mobile station perform beam search in all beam directions, for all $360^\circ \times 360^\circ$ beam pairs [7], [8]. This exhaustive search over all beam pairs would impose significant overhead because of the search complexity involved in selecting the desired beam direction. To reduce the full-scale search involved in the beam sweeping, hierarchical beam-alignment was conceived in [9]–[11]. More particularly, this design relies on multi-resolution codebooks that are employed at different levels. To elaborate further, this technique, which is reminiscent of the binary search algorithm, first involves beam search over a low-level codebook associated with wider beams, then another beam search is followed in the high-level codebook which is a subset of the wide beam selected in the lower level [12]. Unfortunately, the hierarchical codebook based beam-alignment does not reduce the search complexity significantly [12]. Other work that aims for reducing the search complexity involves optimization techniques [13], [14]. However, these methods are only beneficial when the objective function exhibits smoothness. In other words, these techniques only work well for objective functions which have no local optimum.

To reduce the overhead and search complexity involved in the beam-alignment, Nitsche [15] *et al.* proposed blind beam steering relying on accurate location information. More

The fiscal support of InterDigital as well as of the European Research Councils Advanced Fellow Grant under the QuantCom project and of the Royal Society's Global Challenges Research Fund is gratefully acknowledged.

explicitly, the authors proposed a technique by inferring the line-of-sight (LOS) direction between the communicating devices. In this method, the legacy frequency of 2.4GHz/5GHz is used to exploit the channel characteristics. Furthermore, Va *et al.* [4] advocated a beam switching strategy by invoking the classic gradient descent method to maximize the rate under the assumption that the channel always exhibits a single dominant LOS path. However, these methods may not be feasible in practice when the LOS path ceases to exist, which is often the case during heavy traffic, where the dominant LOS path is blocked by the obstacles [3].

To circumvent the necessity of LOS paths, Capone *et al.* [17] conceived context information based beam-alignment, where the BS searches in the context information based direction. This algorithm was then further enhanced with the aid of sophisticated learning techniques [18]. However, this method works well only under the premise that omni-directional reception is employed at the receiver, which makes it impractical for mmWave communications. Moreover, when the LOS is blocked, there may be a set of other possible AoAs/AoDs for steering the beam in the desired location which do not suffer from blockages under a given vehicular traffic density. This approach is considered in [16], [19], where the authors adopt the concept of fingerprint/database from the localization literature. There is a vast body of literature on fingerprint based localization techniques [20]–[24], where typically the channel state information or received signal strength (RSS), which are referred to as fingerprints, are used at pre-determined locations for determining the vehicle's position [20], [21]. To elaborate further, in this treatise, fingerprints are collected for different locations and stored in a database. In this context, the beam pairs (AoA-AoD) are used as a fingerprint to construct the database for different locations. However, a limiting factor of this design is that the fingerprints of the database are fixed for a given location. This is, however, generally not true in the context of beam-alignment, since the beam pair may change depending on the traffic density [25]. In other words, the fingerprint used for a specific traffic density in a given location may be different for another traffic density in the same location.

On the other hand, more recently, machine learning aided wireless transmission has gained attention owing to its more accurate predictions and superior performance over conventional methods dispensing with learning [26]. The state-of-the-art designs in localization literature are predominantly focused on learning [22]–[24]. More particularly, learning based approaches in localization have been shown to be more effective in terms of minimizing the location error. Wang *et al.* [27] demonstrated experimentally that a CSI-based fingerprint relying on deep learning achieves better performance than its counterparts. Capone *et al.* [18] employed a rudimentary learning technique for obstacle avoidance aided cell discovery for beam-alignment. An experimental study on indoor localization conducted by Chen *et al.* [28] attributed its superior performance to learning, where the authors invoke a invoke a convolutional neural network assisted learning scheme.

Motivated by this, in this paper, we employ learning aided beam-alignment, where the learning is invoked for intelligently selecting the fingerprints by invoking a feedforward neural network, namely the softmax linear classifier [29]. In wireless communication systems, the K-nearest neighbors (KNN), support vector machines (SVM), and neural networks are widely used [30]. It is instructive to note that any learning algorithm involves two phases — the training phase, which is carried out offline; and the testing phase, which is carried out in real time. In the KNN algorithm, the training samples are collected and stored in memory during the offline phase, while the nearest neighbors for the observed data are computed and then a decision is made. On the other hand, the SVM relies on a kernel which is a function of feature sets. However, the SVM imposes a high computational complexity when the classifiers are not linearly separable. In contrast to KNN and SVM, the training weights can be determined in the case of neural network assisted learning during the training phase. These weights are then used in real time for prediction or for the selection of fingerprints. Note that unlike the KNN, this method does not require any memory storage for the training samples, since they can be discarded after the training weights have been determined.

Against this background, Table I contrasts our design to state-of-the-art. More explicitly, our contributions in this paper are summarized as follows.

- We propose a multi-fingerprint based database, where the fingerprints are collected for different traffic densities in a given location. Then, the BS intelligently chooses the fingerprint based on the traffic density and location information, where we invoke deep learning for the selection of the fingerprint. More explicitly, we invoke a feedforward neural network, namely the softmax classifier, where the training weights are designed offline for the selection of the fingerprint. Upon the selection of the fingerprint, the BS then relays the information of the fingerprint selected to the mobile station using the legacy frequency. Thereafter, the BS starts the training process to select the beam-pair from the fingerprint which meets the target received signal power. The mobile station feeds back the index of the beam-pair from the selected fingerprint if it meets the threshold. This significantly reduces the search complexity involved.
- We propose a multi-functional beam transmission scheme as an application example of our proposed design, where multiple beams that satisfy the target received power are selected. Then, depending on the mobile station's requirement, the BS can leverage the additional beams for increasing the multiplexing/diversity gains. Furthermore, if the number of RF chains is lower than the number of beam pairs available that meets the target receiver power, the BS then employs beam index modulation to increase the spectral efficiency.
- We demonstrate by our simulations that having multiple fingerprint-based beam-alignment provides a superior performance over the single fingerprint based beam-alignment. Furthermore, we show that our learning-aided multiple fingerprint design provides better fidelity than that of the scheme employing multiple fingerprints

TABLE I. Summary of our design contrasting with state-of-the-art, where ✓and the blank correspond to with and without contributions, respectively .

Themes of Contributions	This Paper	[16]-2018	[11]-2017	[15]-2015	[13]-2014
Beam-Alignment	✓	✓	✓	✓	✓
Intelligence	✓				
Multi-functional Beam Transmission	✓				
Lower Complexity	✓	✓			
Fidelity	✓		✓		
Fingerprints Based	✓	✓			
Fingerprints Adaptation	✓				

but dispensing with learning. Additionally, our proposed learning-aided reduced-complexity beam-alignment design performs similarly to beam-sweeping based beam-alignment relying on high-complexity exhaustive beam-search. More explicitly, our design is capable of maintaining the target RSS in dense vehicular environments, while both single fingerprint and line-of-sight (LOS) based beam-alignment suffer from blockages.

The rest of the paper is organized as follows. In Section II, we detail the system model of fingerprint based beam-alignment in mmWave communication, while in Section III we present our proposed deep learning assisted beam-alignment relying on multi-fingerprint database design to achieve near-perfect beam-alignment. Section IV and Section V presents our simulation results and complexity discussion, followed by our conclusions in Section VI.

Notations: We use upper case boldface, $\mathbf{A}$, for matrices and lower case boldface, $\mathbf{a}$, for vectors. We use $(.)^T$, $(.)^H$, $\|.\|_{\mathrm{F}}$, $\mathrm{Tr}(.)$ $\mathbb{E}(.)$ for the transpose, Hermitian transpose, Frobenius norm, trace and expectation operator, respectively. We adopt $\mathbf{A}(m,n)$ to denote the m^{th} row and n^{th} column of the $\mathbf{A}$, $\mathbf{I}_N$ is the identity matrix of size $N \times N$, and $\mathbf{A} \succ 0$ indicate that $\mathbf{A}$ is a positive definite matrix. Finally, we use $\mathcal{CN}$, $\mathcal{U}$, and i.i.d. to represent complex-valued normal distribution, uniform distribution, and independent and identical distribution, respectively.

II. System Model

Let us consider a vehicular scenario, where a BS serves the vehicles (users) of its cell. The number of vehicles N_v at any point of time obeys the Poisson distribution with a mean of λ and variance of λ. Let us also assume that the serving cell is partitioned into N locations, where the BS is equipped with the knowledge of the fingerprints (FP) for each location in its database, as shown in Fig. 1. In this paper, we define fingerprints as beam-pairs, whose AoA-AoD values are pre-determined offline. We refer the readers to [20], [21], [31] for a detailed account on fingerprint based communication. Fingerprints, i.e. AoA-AoD pairs in our design, are typically obtained by employing beam-sweeping, where a high-resolution scanning of beam-pairs is carried out. However, given the time-varying traffic density, corresponding to the varying number of vehicles at any point of time, a single pre-determined fingerprint would not be able to provide improved performance at a reduced search complexity. This is because the AoA-AoD pair which provides high received signal power may be blocked/suppressed by the neighboring vehicles. Hence a multi-fingerprint based regime is conceived for different traffic densities at a given location.

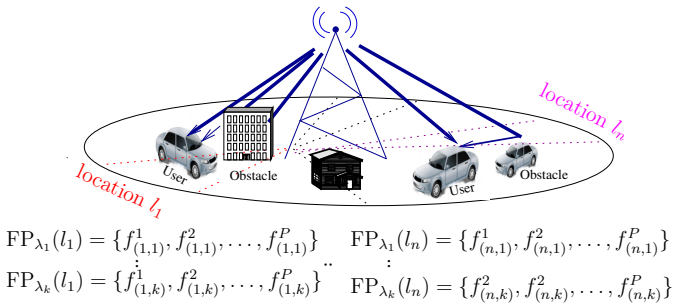

Fig. 1. Fingerprint Based beam-alignment.

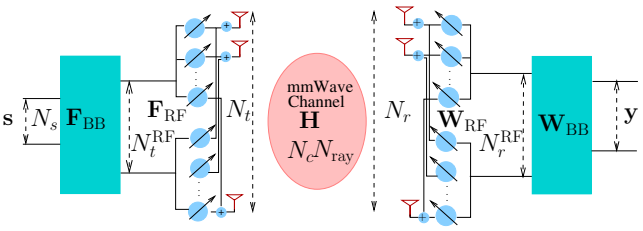

Fig. 2. Hybrid beamforming architecture.

Fig. 1 shows our system model, where the BS is serving a user in location l_1 for a traffic density λ_k using the fingerprint $\mathrm{FP}_{\lambda_k}(l_j)$[1], where the entry $f^i_{k,j}$ denote the i^{th} fingerprint at j^{th} location for traffic density k. Furthermore, owing to the hardware complexities and power hungry ADCs/DACs at mmWave frequencies, dedicating an RF chain to each and every antenna element would become impractical; and employing analog only beamforming would result in poor angular resolution and inaccuracies. Therefore, a hybrid beamforming solution is conceived by the amalgamation of both digital and analog beamforming [32]–[34]. More explicitly, in a hybrid beaforming design, the signals are digitally precoded in the baseband and then phase-shifted in the RF stage by analog phase shifters [33], [34]. The state-of-the-art hybrid beamforming architectures tend to rely either on fully-connected or on sub-array-connected [2]. In the fully-connected design, each RF chain is connected to all the phase shifters of the antenna array as shown in Fig. 2. By contrast, in the sub-array-connected design, the antenna array is partitioned into

[1]The location information may be obtained from the global positioning system (GPS).

sub-arrays, where each RF chain is connected to only a subset of the phase shifters [2]. Similarly, in our design, the BS and the user may employ either fully-connected or sub-array connected designs for achieving beamforming gains. However, as design example, we assume that both the BS and the user employ the fully-connected architecture shown in Fig. 2, where the signals are precoded digitally using the matrix $\mathbf{F}_{\text{BB}}$ in the baseband and then phase-shifted by the analog RF beamforming matrix $\mathbf{F}_{\text{RF}}$.

Let us now consider that the BS (transmitter) is equipped with N_t transmit antennas and N_t^{RF} chains, while the user (receiver) is equipped with N_r receive antennas and N_r^{RF} chains. Furthermore, let us assume that $\{(\mathbf{f}_{\text{RF}}^1, \mathbf{w}_{\text{RF}}^1), (\mathbf{f}_{\text{RF}}^2, \mathbf{w}_{\text{RF}}^2), \ldots, (\mathbf{f}_{\text{RF}}^N, \mathbf{w}_{\text{RF}}^N)\}$ are chosen as the beamforming vectors at the BS and at the user end, respectively, for a traffic density of λ. Then the received signal vector at the user is given by

$$\mathbf{y} = \sqrt{P_t}\mathbf{W}_{\text{BB}}^H\mathbf{W}_{\text{RF}}^H\mathbf{H}\mathbf{F}_{\text{RF}}\mathbf{F}_{\text{BB}}\mathbf{s} + \mathbf{W}_{\text{BB}}^H\mathbf{W}_{\text{RF}}^H\mathbf{n}, \quad (1)$$

where $\mathbf{F}_{\text{RF}}$ is the transmit beamforming matrix of size $N_t \times N_t^{\text{RF}}$ at the BS, where N_t^{RF} columns are constructed from the potential AoD set $\{\mathbf{f}_{\text{RF}}^1 \ldots \mathbf{f}_{\text{RF}}^N\}$. Similarly, $\mathbf{W}_{\text{RF}}$ is the receive beamforming matrix of size $N_r \times N_r^{\text{RF}}$ at the user end, where N_r^{RF} columns are constructed from the potential AoA set $\{\mathbf{w}_{\text{RF}}^1 \ldots \mathbf{w}_{\text{RF}}^N\}$. Furthermore, $\mathbf{s}$ is the transmitted symbol, $\mathbf{n}$ is the noise vector of identical and independent distributed entries with distribution $\mathcal{CN}(0, \sigma^2\mathbf{I})$, while $\mathbf{H}$ is the statistical mmWave channel model of size $N_r \times N_t$ expressed as

$$\mathbf{H} = \sqrt{\frac{N_r N_t}{N_c N_{\text{ray}}}} \sum_{n_c=1}^{N_c} \sum_{n_{\text{ray}}=1}^{N_{\text{ray}}} \alpha_{n_c}^{n_{\text{ray}}} \mathbf{a}_r(\phi_{n_c}^{n_{\text{ray}}}) \mathbf{a}_t^T(\phi_{n_c}^{n_{\text{ray}}}), \quad (2)$$

while $\alpha_{n_c}^{n_{\text{ray}}} \sim \mathcal{CN}(0,1)$ is a complex-valued Gaussian random variable, whose amplitude and phase are Rayleigh and uniformly distributed, respectively. For a uniform linear array (ULA) having N_r and N_t antenna elements the response vectors $\mathbf{a}_r$ and $\mathbf{a}_t$ are expressed as

$$\mathbf{a}_r(\phi_r) = \frac{1}{\sqrt{N_r}}[1 \; e^{j\frac{2\pi}{\lambda}d\cos(\phi_r)} \ldots e^{j\frac{2\pi}{\lambda}(N_r-1)d\cos(\phi_r)}]^T, \quad (3)$$

$$\mathbf{a}_t(\phi_t) = \frac{1}{\sqrt{N_t}}[1 \; e^{j\frac{2\pi}{\lambda}d\cos(\phi_t)} \ldots e^{j\frac{2\pi}{\lambda}(N_t-1)d\cos(\phi_t)}]^T, \quad (4)$$

where ϕ_r and ϕ_t are the angles of arrival and departure, respectively.

In this paper, we consider the received signal strength[2] (RSS) [35] as the performance metric to determine the beam-pair for a successful transmission. Furthermore, for the construction of the fingerprints database, we accounted for the attenuation and blockage caused by neighboring vehicles in addition to the path loss experienced by the mmWave carrier. To achieve this, we have invoked the multiple knife-edge model recommended by ITU-R [36]. For a given location, each fingerprint is constructed for each traffic density, by accounting for the total attenuation caused by the vehicles. The attenuation caused by each vehicles using single knife-edge is given by [3], [36]

$$A = \begin{cases} 6.9 + 20\log_{10}\left[\sqrt{(v-1)^2+1} + v - 0.1\right], \forall v > -0.7 \\ 0 \qquad \text{Otherwise,} \end{cases} \quad (5)$$

where $v = \sqrt{2}h/r_f$, h is the height of the obstacle from the line joining the BS and the user, and r_f is the Fresnel ellipsoid radius expressed as

$$r_f = \sqrt{\frac{\Lambda d_{\text{obstacle}} d_{\text{user}}(d_{\text{user}} - d_{\text{obstacle}})}{d_{\text{user}}}},$$

where Λ is the wavelength, d_{user} is the distance between the transmitter and user, while d_{obstacle} is the distance between the transmitter and an obstacle as shown in Fig. 3.

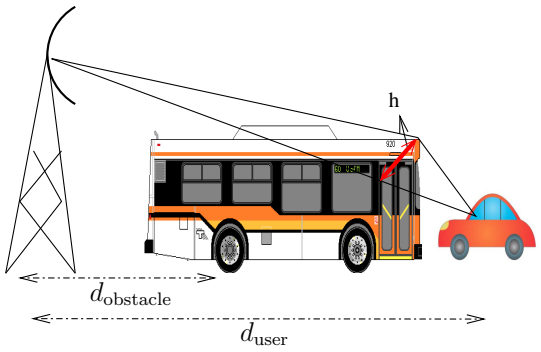

Fig. 3. Knife-edge diffraction caused by the vehicle obstacle.

On the other hand, the path loss experienced by the signal at a distance of d for a transmit and receive antenna gain of G_t and G_r, respectively, is given by [1]

$$PL_{[dB]} = PL_0 + 10n_p \log\left(\frac{d}{d_0}\right) + S_{\sigma_s} + G_t + G_r, \quad (6)$$

where d_0 is the close-in reference distance, S_{σ_s} is the shadowing factor, while PL_0 is the free-space path loss. Furthermore, for a given wavelength (Λ) the free-space path loss is expressed as

$$PL_0 = 20\log_{10}\left(\frac{4\pi d_0}{\Lambda}\right).$$

Therefore, the total received power after accounting for both the path loss and the attenuation caused by a vehicle is

$$P_r = P_t - PL_{[dB]} - A. \quad (7)$$

It is instructive to note that (7) is due to large scale fading. However, considering the small scale fading as well as the beamforming and combining effects, the net received power $P_{r_{\text{net}}}$ is expressed as

$$P_{r_{\text{net}}} = P_r + 10\log_{10}\left\|\left(\mathbf{W}_{\text{BB}}^H\mathbf{W}_{\text{RF}}^H\mathbf{H}\mathbf{F}_{\text{RF}}\mathbf{F}_{\text{BB}}\right)\right\|_{\text{F}}^2, \quad (8)$$

while the capacity is given by

$$C = \quad (9)$$

[2]Note that other performance indicators may also be used, such signal-to-noise ratio (SNR), rate, received signal quality (RSQ).

$$\log_2\left(\mathbf{I}+P_r\mathbf{Z}^{-1}\left(\mathbf{W}_{\mathrm{BB}}^H\mathbf{W}_{\mathrm{RF}}^H\mathbf{H}\mathbf{F}_{\mathrm{RF}}\mathbf{F}_{\mathrm{BB}}\right)\left(\mathbf{W}_{\mathrm{BB}}^H\mathbf{W}_{\mathrm{RF}}^H\mathbf{H}\mathbf{F}_{\mathrm{RF}}\mathbf{F}_{\mathrm{BB}}\right)^H\right) \tag{10}$$

where $\mathbf{Z} = \sigma_n^2\left(\mathbf{W}_{\mathrm{BB}}^H\mathbf{W}_{\mathrm{RF}}^H\right)\left(\mathbf{W}_{\mathrm{RF}}\mathbf{W}_{\mathrm{BB}}\right)$, σ_n^2 is the noise variance. The net received power $P_{r_{\mathrm{net}}}$ is observed for the fingerprint construction. A beam sweeping action is carried out initially for N locations at discrete traffic densities and then the specific beam-pairs which achieve the target RSS are stored in the database. In other words, the AoA-AoD fingerprint is obtained by conducting a high-resolution beam-search campaign by accounting for all blockages caused by obstacles. The fingerprint construction is typically carried out offline either by computer-generated environment simulations, or in real time during the BS installation.

In the next section, we discuss multi-fingerprint construction as well as the learning assisted fingerprint adaptation, followed by multi-functional beam transmission.

III. Proposed Design

In this section, we commence by outlining our multi-fingerprint based beam-alignment, where we propose multiple fingerprints for a given location for different traffic densities. Then, we aim for improving the design by adopting a learning based approach for fingerprint adaptation followed by a discussion on the concept of multi-functional beam transmission, where a plurality of beam-pairs satisfying the RSS threshold are selected for attaining both multiplexing and diversity gains. Furthermore, we also propose that if the number of beams are higher than the number of RF chains, beam index modulation is employed to attain a high spectral efficiency.

A. Multi-Fingerprint Based Beam-Alignment

Achieving accurate beam-alignment in directional transmission systems is challenging, especially at mmWave frequencies because of its high susceptibility to blockages. To circumvent this problem a fingerprint based beam-alignment technique may be employed. In broader terms, having accurate fingerprint may be viewed as side-information, which is used for enhancing the system performance. In our design, the fingerprint is comprised of a set of possible beam-pairs for a given location, over which a communication link can be established. Typically, a fingerprint is constructed for each location during the BS installation stage by taking the surrounding environment into account, such as buildings, lamp posts, vehicles, etc. However, the ever-changing vehicular traffic may strictly limit the performance of the fingerprint. This is because the direction of the beam or the number of beam-pairs available is highly dependent on the density and position of vehicles on the road. In other words, it depends on the traffic density. Furthermore, the traffic density is time-varying. For example, the traffic density in the morning is different from that in the afternoon, or during special events. This necessitates using multiple fingerprints for a given location, depending on the traffic density. A typical multi-fingerprint based database is shown in Table II, where BP_2 represents a legitimate angle of departure, say AoD ($=30^\circ$), whose corresponding angle of arrival pair may be say, AoA ($=60^\circ$), indexed as beam-pair 2 (AoD-AoA). Similarly, BP_{10} denotes beam pair 10, whose angles of departure and arrival may be 110° and 270°, respectively. By generalizing, BP_X denotes the beam pair of any angle of departure paired with the corresponding angle of arrival, denoted by index X. It is constructed by calculating the net received power using (7) for each location at different traffic densities. It is interesting to note that this multi-fingerprint adaptation is akin to the classical link-adaptation involving multiple modulation coding scheme (MCS), bit error ratio (BER) and SNR, where the transmitter adapts among different schemes to provide high data rates under given channel conditions while also meeting the target BER.

TABLE II. An example illustrating multi-fingerprint database

Location	Traffic Density	Beam-Pairs (BP)
L_1	λ_1	$BP_2, BP_{10}, BP_{23}, \ldots$
L_1	λ_2	$BP_{320}, BP_{210}, BP_3, \ldots$
$\vdots$	$\vdots$	$\vdots$
L_k	λ_1	$BP_1, BP_9, BP_{300}, \ldots$
$\vdots$	$\vdots$	$\vdots$
L_n	λ_3	$BP_{21}, BP_6, BP_{250}, \ldots$

This relationship can be represented by a look-up table for link-adaptation, where depending on the traffic density and on the location, its corresponding fingerprint is selected. For example, if the user is at the location L_1 and the BS estimates the traffic density as λ_2, then the BS selects the fingerprint consisting of beams $\{BP_{320}, BP_{210}, BP_3, \ldots\}$. The BS then shares this information with the user, whereupon the BS and user invoke training for identifying the best beam-pair amongst the available beam-pairs of the fingerprint selected. This significantly reduces the search space involved in the beam-alignment. To further reduce the search complexity, a RSS threshold is set, where the user selects the specific beam-pair whose observed RSS value is higher than the threshold. Having selected the beam pair, the user relays this information to the BS, eliminating the search over the successive beam-pairs. While this procedure is different for transmission over a plurality of beam-pairs invoked in order to achieve diversity or spatial multiplexing gains, where the search is continued until the required number of beam-pairs are found.

However, given the ever-changing nature of the channel and the non-linearities imposed by the analog-to-digital and digital-to-analog converters (ADC/DAC) which is even more pronounced at mmWave frequencies, a look-up table assisted fingerprint adaptation would be significantly affected, which we will discuss in the simulation results.

Remark: The fingerprints can be constructed empirically offline during the network design stage. It is important to note that the construction of the fingerprints depends on the topology of the road structure and buildings, which are static and hence do not change within short time scales – this may change if a new building is erected. The changes in the environment are attributed to the ever-changing vehicular traffic. In other words, in the absence of traffic, the fingerprints

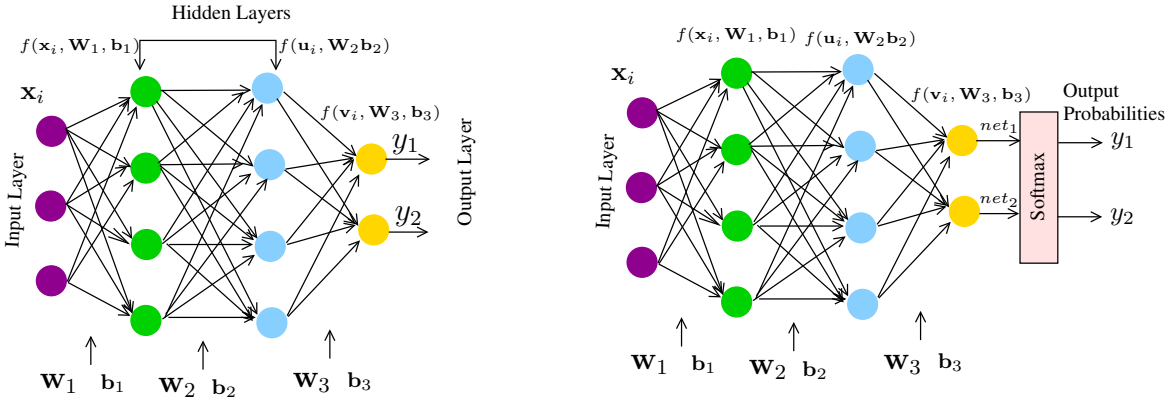

(a) A typical neural network.

(b) A softmax feedforward neural network.

Fig. 4. Architecture of a neural network.

constructed during the network design stage would hold indefinitely, unless the area topology changes. However, because of the time-varying vehicular density, the number of possible beam-pairs may be subject to change. Therefore, it is possible to construct the fingerprints for different traffic densities by allowing the vehicles, to identify the potential beam-pairs by conducting beam-sweeping during the beam-pair training phase. This process can be repeated for different vehicular densities. Furthermore, the number of fingerpints required is location specific and can be empirically determined.

B. Learning-Aided Multi-Fingerprint Based Beam-Alignment

We have discussed in the previous section that a multi-fingerprint based beam-alignment would account for beam-pairs that are capable of handling different traffic densities, where the BS selects the fingerprint that is pertinent to the traffic density and location observed. This is carried out relying on a look-up table. However, while this design enhances the performance compared to that of a single fingerprint based beam-alignment, the performance gain may become limited if the threshold values, such as RSS observed in a fingerprint at a given location L for a traffic density λ of the look-up table becomes outdated. In other words, the performance of a look-up table based fingerprint adaptation may limit the performance because of the uncertainties mentioned in Sec. III-A, and hence it becomes extremely challenging to attain perfect beam-alignment. Therefore, we resort to a learning-aided multi-fingerprint based beam-alignment. The rationale for employing learning is to eliminate the dependence on traffic density threshold values, as enumerated in Table II during the fingerprint selection. This is because, the values may become outdated owing to the imperfections in the channel and impairments in the ADC/DACs.

Therefore, in this paper, we conceive a neural network based approach for intelligent adaptation between multiple fingerprints. The rationale for choosing a neural network is its reduced complexity while providing a superior performance. The learning approach pursued in this paper relies on two stages: the training phase and the testing phase. In the training phase, the weight vectors of the network are computed using training samples, where the input and output are known. This is classified as a supervised learning technique, where the training weights are designed using supervision. It is instructive to note that the training weights are calculated offline, hence this calculation does not impose any real time overhead on the system. A typical neural network is shown in Fig. 4a.

This network is referred to as a deep neural network if the number of hidden layers is higher than one, as shown in Fig. 4a, where the number of hidden layers is two. As seen in the figure, the training samples are passed to the input layer and the weights are designed for minimizing the error, which is the difference between the true and predicted output values. In Fig. 4a, $\mathbf{W}_1, \mathbf{W}_2$, and $\mathbf{W}_3$ are the weights for the input layer, hidden layer, and output layer, respectively, where $\mathbf{W}(p, q)$ denotes the weight attached between the nodes p and q, while $\mathbf{x}_i, \mathbf{u}_i, \mathbf{v}_i$ and y_1, y_2 are the inputs and outputs of the network, respectively, where i denotes the class. In our design, each fingerprint corresponds to a class. Furthermore, the output of each hidden layer is defined by an activation function $f(.)$, also called a score function, which determines the performance of the system. The choice of the activation function is dependent on the analytical tractability, computational complexity and the type of output signal. On the other hand, to yield better results, a loss function is introduced which captures the error (loss) between the predicted outcome and the real outcome in the training samples.

In our proposed design, the choice of the fingerprint (or class) is dictated by the output probabilities associated with each fingerprint. In other words, the fingerprint having a high probability is selected. Since we deal with the probabilities at the output, it can be interpreted as a logistic regression having multiple classes, where each fingerprint constitutes a class. Hence, an activation (score) function which deals with the probability is considered, where in our case we use a so-called softmax function, which we will discuss in detail later in this section. The resultant neural networks are also sometimes referred to as softmax neural network [29].

Each layer of Fig. 4a is assigned a score by the activating function. However, since we deal with the probabilities of spe-

cific outcomes, the linear weights are translated to probabilities by a softmax function at the output, as shown in Fig. 4b and expressed as [29]

$$f_i(z) = \frac{e^{z_i}}{\sum_k e^{z_k}}, \tag{11}$$

where z is the score vector at the layer before the output probabilities are calculated, which is given by [29]

$$z = f(\mathbf{x}_i, \mathbf{W}, b) = \mathbf{W}\mathbf{x}_i + \mathbf{b}. \tag{12}$$

In (12) $\mathbf{W}$ is the weight matrix of the layer, $\mathbf{b}$ is the bias vector, while $\mathbf{x}_i$ is the input of the layer, as shown in Fig. 4b. As an example, let us consider Fig. 4b, where the softmax function is applied at the output layer to the scores net_1 and net_2, which are calculated using the weight matrix $\mathbf{W}_3$ and bias vector $\mathbf{b}_3$. Note that the softmax function is employed only at the output layer, while for all other layers, only the scores attained using (12) are calculated as shown in Fig. 4b.

In our paper, the input vector $\mathbf{x}_i$ is a three-dimensional vector holding the location, traffic density and RSS values, while the output represents the probabilities associated with each fingerprint. In other words, the output takes the form of $[0\ldots,0,1,0,\ldots,0]^T$, where 1 is the probability associated with that particular fingerprint.

It is instructive to note that the weight matrices are initially chosen as random from the distribution $\mathcal{N}(0,1)$, hence the prediction at the output would be erroneous. Therefore, to improve the prediction of the fingerprint for a given traffic density and location, a loss function is introduced which is a measure of difference between the predicted probability and the true probability associated with the given class. In other words, by considering the loss function, the weight matrices are optimized for ensuring the loss is minimized. More explicitly, in our design we aim for minimizing the divergence between the real and predicted probability distributions. This loss function can also be interpreted as the Kullback-Leibler divergence between two distributions. Thus, for distributions p and q it is expressed as [37]

$$D_{KL}(p\|q) = -\sum_S p(i)\log q(i), \tag{13}$$

where in our case, $p(i)$ is the probability of the correct class i, which is $p(i) = [0,\ldots,1,\ldots,0]$, while q is the function in (11). Upon substituting (11) into (13), we get

$$D_{KL}(p\|q) = -\sum_S \log \frac{e^{z_i}}{\sum_k e^{z_k}}, \tag{14}$$

where S is the number of training samples.

Additionally, we have the cross-entropy of $\mathcal{H}(p,q) = \mathcal{H}(p) + D_{KL}(p\|q)$, where $\mathcal{H}(p) = 0$ holds, since there is no uncertainty in the correct class. Therefore, this loss function may also be referred to as cross-entropy loss.

Having defined the cross-entropy loss[3], the total loss function over all classes associated with a regularization penalty of $R(\mathbf{W})$ is given as [29]

$$L = -\frac{1}{S}\sum_s \log \frac{e^{z_i}}{\sum_k e^{z_k}} + R(\mathbf{W}), \tag{15}$$

where we have $R(\mathbf{W}) = \frac{\lambda}{2}\|\mathbf{W}\|_2^2$ and S is the total number of training samples. The rationale behind adding a regularization term in (15) is to ensure that it does not result in over-fitting [29].

We now aim for minimizing (15) by computing the gradient with respect to the weight matrix $\mathbf{W}_3$ and the bias $\mathbf{b}_3$ of Fig. 4b. To achieve this, we compute the gradient for each class whose weights are now w_3^i and bias b_3^i, where i represents the class. Note that z_i in (15) is a function of the weight matrix $\mathbf{W}_3$ and bias vector $\mathbf{b}_3$. After a series of steps, the gradient with respect to W_i and b_i is given as [29]

$$\frac{\partial L}{\partial \mathbf{w}_3^i} = (f_i - \delta_{ik})\mathbf{x} + \lambda \mathbf{w}_i \quad \delta_{ik} = \begin{cases} 1, i = k \\ 0, \text{otherwise} \end{cases} \tag{16}$$

$$\frac{\partial L}{\partial b_3^i} = f_i - \delta_{ik}. \tag{17}$$

Thus, by employing gradient-descent we arrive at

$$\mathbf{w}_3^i = \mathbf{w}_3^i - \alpha\frac{\partial L}{\partial \mathbf{w}_3^i}, \tag{18}$$

$$b_3^i = b_3^i - \alpha\frac{\partial L}{\partial b_3^i}, \tag{19}$$

where α is the step-size. Similarly, weight matrices $\mathbf{W}_1$ and $\mathbf{W}_2$, and bias vectors $\mathbf{b}_1$ and $\mathbf{b}_2$ are obtained by employing the gradient of the loss function in (16) with the respective matrix $\mathbf{W}$ and vector $\mathbf{b}$. This process is called as error backpropagation [29]. The pseudo-code of the proposed learning-aided fingerprint based algorithm is presented in Algorithm 1.

It is important to emphasize that the weight matrix $\mathbf{W}$ and bias vector $\mathbf{b}$ of the network are computed offline and stored in memory. This entire process is carried out during the training phase.

Having discussed the softmax training phase, we now focus our attention on the real time, the testing phase. During the initial access the BS communicates with the user by employing omni-directional transmission using lower frequencies such as that of LTE, where the BS estimates the location of the user. The BS also has the information of the number of users (vehicles) in its cell, which is exploited for estimating

[3]In our papaer, we employed supervised learning, where the training labels, i.e., the output samples corresponding to the input samples are known, which is then used to calculate the loss function. For example, if the loss function used is the mean-squared error (MSE), then the error between the predicted output (label) and the actual label (known output during the training) is computed. This error is then used for desiging the neural network weights. In our case, since the output is the probability of the fingerprint FP, we invoke the cross-entropy as the error function instead of the MSE. In other words, the cross-entropy function quantifies the probabilistic-distance, i.e., the Kullback-Leibler divergence between the predicted probability of the actual label and the actual probability associated with that label (Note: since this is a training sample and is known apriori, the actual probability of that training label is 1.).

Algorithm 1 Proposed Learning-Aided beam-alignment

Offline:

1: Input: Training samples for all training locations
2: Output: Fingerprint
3: Initialize $\mathbf{W}_1$, $\mathbf{W}_2$ and $\mathbf{W}_3$ as random
4: Compute the output of $f(.)$ using (12) for each layer with the assigned weights
5: Apply softmax function using (11) to obtain the probabilities for each class
6: Obtain the weight matrices and bias vectors by (18) and (19)
7: Do error backpropagation
8: Repeat 4-7 until convergence of (16).

Online:

1: Input the location, number of vehicles, Target RSS
2: Apply training weights found during offline phase
3: Output: desired fingerprint

the vehicular density (λ). Furthermore, the user relays the information of its RSS threshold requirements to the BS. Given the number of vehicles, the RSS threshold, and the location as the input parameters, the BS employs the softmax algorithm with the weights and bias calculated during the training stage. The algorithm then predicts the probability of each class, i.e. each fingerprint, and then the BS selects the fingerprint having the highest probability. After the selection of the fingerprint, it informs the user about the possible beam-pairs, and conducts beam-search over these selected beam-pairs. The user then feeds back the specific beam-pair index which meets its post-processing RSS threshold. A schematic diagram illustrating the algorithm is shown in Fig. 5.

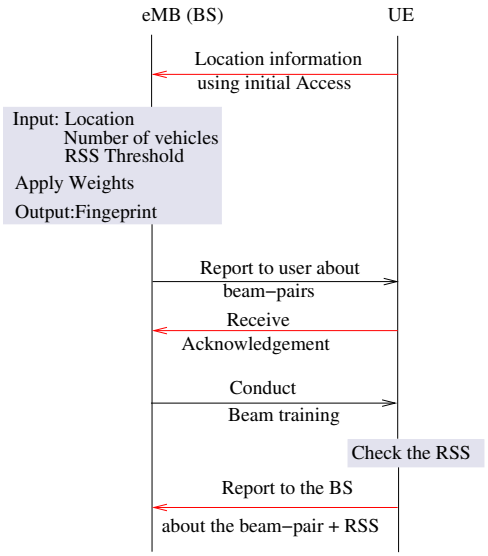

Fig. 5. The beam-alignment procedure.

In the next section, we present our multi-functional beamforming as an application of the proposed design.

C. Application: Multi-functional Beam Transmission

In this section, we propose a multi-functional beam transmission by allowing some tolerance in the beam search complexity. The rationale for employing multi-functional beam transmission is to increase the spectral efficiency as well as to enhance the performance. This philosophy works under the assumption that there exist a plurality of beam-pairs which satisfy the RSS threshold. As discussed in Sec. III-A and Sec. III-B, the BS conducts beam-search in the selected fingerprint, where the user chooses the specific beam-pair which satisfies the target RSS and feeds back the index of the beam-pair to the BS using LTE and avoids the beam search in the successive beam-pairs.

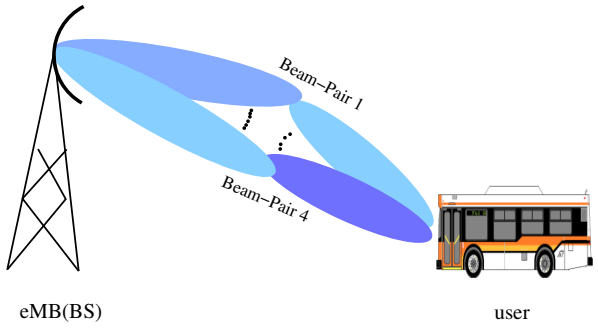

Fig. 6. A plurality of beam-pairs selected to attain diversity/multiplexing gains.

By contrast, in the multi-functional beam transmission, the user chooses several beam-pairs which satisfies the RSS threshold at the expense of increased search complexity[4] as shown in Fig. 6. Additionally, in this scenario, the beam-pair search complexity can be reduced by invoking the tabu search algorithm proposed by Gao *et al.* [38].

These additional beam-pairs can be leveraged to achieve diversity and/or multiplexing gains. It is important to emphasize that the number of beams that can be exploited is limited by the number of RF chains. Given the eligible beam-pairs observed, the BS-user pair may also employ link-adaptation depending on the nature of the channel in each beam. In other words, depending on the post-processing SNR observed at the user, the BS may employ diversity or multiplexing. Explicitly, if the channel is in deep fade, the user may opt for employing diversity, whilst for multiplexing otherwise. Furthermore, the BS may also optimize the power allocation for each beam in conjunction with multiplexing- and diversity-aided transmission.

On the other hand, if the number of beam-pairs observed by the user that satisfy the target RSS is higher than the number of RF chains[5], the BS may decide to employ beam-index modulation[6] using the beam-pairs reported by the user

[4]It is important to emphasize that there may also be a scenario, where there is no an additional beam-pair despite the increased beam search in the successive beam-pairs.

[5]Note that the maximum number of beam-pairs the BS can leverage is equal to the number of RF chains.

[6]Beam-index modulation allows us to convey extra implicit information by inferring at the receiver which specific beam was activated.

as shown in Fig. 7.

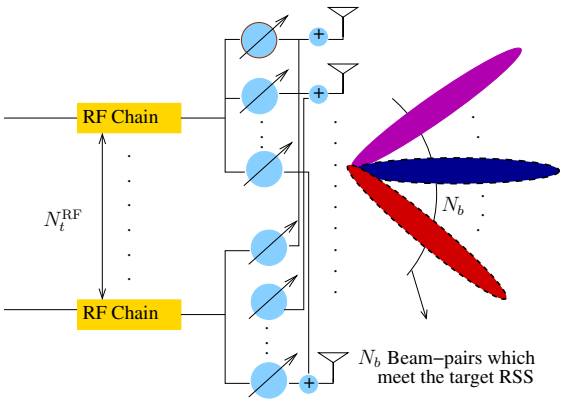

Fig. 7. Beam index modulation at the BS.

Fig. 7 illustrates the typical beam index modulation employed at the BS to increase the data rate. Note that here the number of beam pairs N_b that meets the target RSS is higher than the number of RF chains N_t^{RF}. This is akin to the spatial modulation, where the antenna index carries the information. In contrast to the antenna index in spatial modulation, in this design, beam index is used for the information conveyance. Thus the total number of bits that can be transmitted per second per channel per user is

$$\text{Number of bits} = \underbrace{\log_2 M}_{\text{M-ary bits}} + \underbrace{\log_2 N_b}_{\text{number of beam pairs}} .$$

We note that in addition to the beam-pairs selected for the transmission based on the input signal stream during beam index modulation, diversity or multiplexing gains may also be attained by the selected beam-pairs depending on the channel's nature in these beam-pairs.

In the next section, we present our simulation results of the proposed design.

IV. Simulation Results

In this section, we present our simulation results for characterizing the performance of the proposed design. More explicitly, we characterize the performance of the multi-fingerprint aided beam-alignment scheme relying on learning and of the benchmark design dispensing with learning. In our simulations, the number of vehicles at any point of time follows Poisson distribution $\sim$ Poisson(λ) having both a mean and variance of λ. Furthermore, the blockages caused by vehicles are random obeying the distribution $\mathcal{U}(0, N_v)$, where N_v is the number of vehicles having a Poisson distribution $\sim$ Poisson(λ). At the time of writing, there is no mathematical model or distribution for blockage, only empirical models [3]. Hence, we assumed in our simulations that the maximum number of blockages is equal to the number of vehicles. Furthermore, from the database on the vehicle dimension [39], it was found that the height of the vehicles follows normal distribution with a mean of μ_h and standard deviation of σ_h [3]. Our simulation parameters are summarized in Table III. On the other hand, for the neural network, we have employed two hidden layers with 20 nodes each, while the number of nodes in the input and output layers is 3. Furthermore, the activation function chosen in each hidden layer is a Tan-Sigmoid function, while it is the softmax function in the output layer. In this paper, we have considered multi-fingerprints for three different traffic densities.

TABLE III. Simulation parameters

Parameters	Values
P_t	20 dBm
N_t	32
N_r	8
G_t	10 dBi
G_r	5 dBi
$\Lambda(28\ \text{GHz})$	0.0107
Number of Vehicles (N_v)	Poisson (λ)
Vehicles height [meters]	$\mathcal{N}(150, 8.6)$
Blockages	rand$(0, N_v)$
$d_{\text{user}}, d_{\text{obstacle}}$	rand(.)

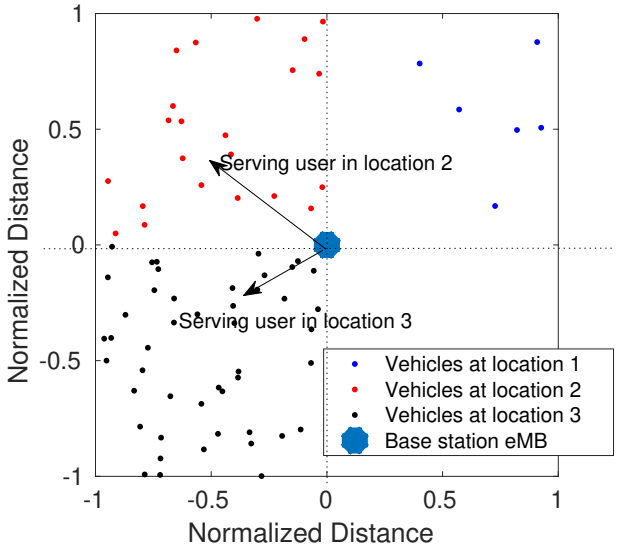

Fig. 8. Distribution of users at four locations.

Fig. 8 shows an example, where a BS is located at the center of the cell. Furthermore, the cell is partitioned into four locations, and each location has its own fingerprints for the different traffic densities. It is important to emphasize that the number of vehicles in each location is Poisson distributed, while the distance of the vehicles from the BS in each cell is uniformly distributed. Observe in Fig. 8 that the BS is serving two users in Locations 2 and 3, while the vehicles near the users are treated as obstacles.

Fig. 9 shows the instantaneous RSS values for three fingerprints, when the number of vehicles is Poisson distributed, as shown in Fig. 8 having means of 5, 20 and 45. More explicitly, Fig. 9a depicts the RSS values for the scenarios, where the difference in the height of the obstacle to the line joining the transmitter and receiver is such that v of (5) is less than -0.7, i.e. the vehicular attenuation is zero. In other words, the attenuation of the signal is purely due to path loss.

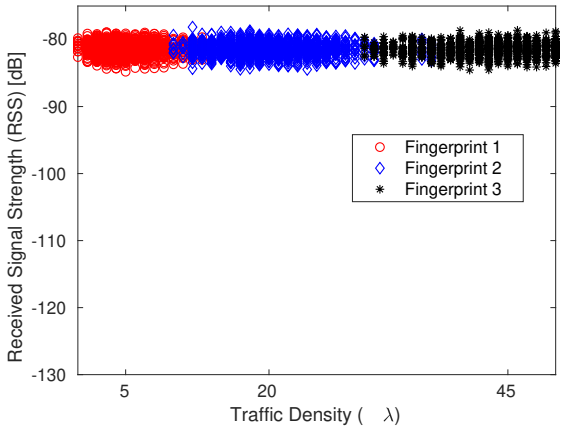

(a) Instantaneous RSS values observed for $v < -0.7$ for three fingerprints at three traffic densities.

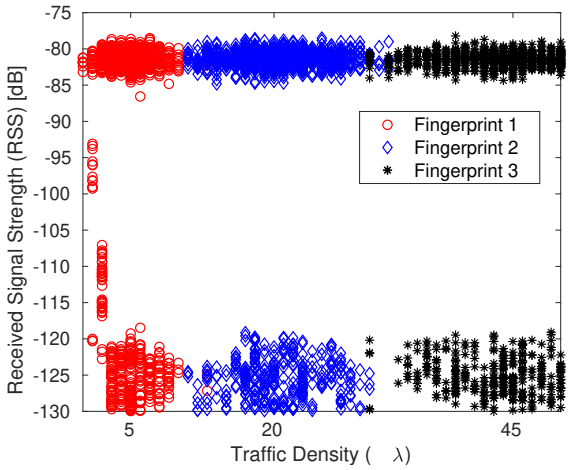

(b)

Fig. 9. Instantaneous RSS values observed for $v < -0.7$ for three fingerprints at three traffic densities.

However, the fluctuations observed in Fig. 9a are owing to the fading introduced by the channel, which is captured in (8).

On the other hand, Fig. 9b depicts the RSS values for the scenario, where the difference in the height of obstacle to the line joining the transmitter and receiver is such that v of (5) is greater than -0.7. In other words, the signal experiences attenuation due to both the vehicles and path loss, which becomes evident from the plot, where there are points scattered around having RSS values as low as -125 dB. The physical meaning of this is that some of the beam-pairs available in the fingerprints are subjected to blockages because of the vehicular obstruction. We note that in the absence of these blockages, Fig. 9b would show similar behavior to Fig. 9a, where both both Fig. 9a and Fig. 9b are plotted for a non-adaptive system.

To analyze the loss function of the softmax neural network presented in (15), Fig. 10 shows the cross-entropy of the network during training versus the number of epochs[7]. It can

[7]The network is said to have reached '1 Epoch' when each and every sample of the data is passed through the network for designing the network parameters for once. Explicitly, the 'epoch' may be loosely defined as the number of times the dataset is used for designing the parameters.

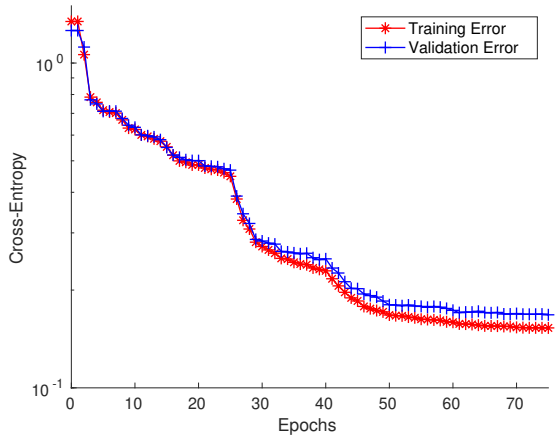

Fig. 10. The training and validation curves of the neural network employed.

be seen from the figure that the network's best performance is reached after approximately 60 epochs. Furthermore, it can be observed from the figure that the validation error is only slightly higher than the training error, which implies that the neural network weights designed are indeed capable of providing a good fit in terms of the mapping between the input and the output samples. It is instructive to note that Fig. 10 can be used to study how well the neural network parameters are designed. In other words, if the validation error in Fig. 10 is high, while the training error is low, this implies over-fitting of the network and hence the regularization parameters may be adjusted; on the other hand, if both the validation and training errors are high, this implies under-fitting and hence the number of neurons (nodes) may be adjusted.

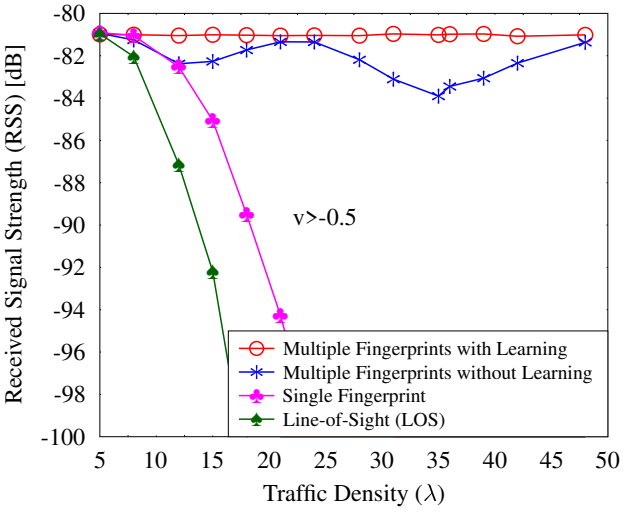

Fig. 11. Received signal strength (RSS) of the different schemes against traffic density.

Fig. 11 shows the RSS observed for a system employing multiple fingerprints both with and without learning, a single

fingerprint as well as for line-of-sight (LOS)[8] propagation. In this simulation, we have set the target RSS to -82 dBm. It is evident from Fig. 11 that multiple fingerprint based beam-alignment provides superior performance, while the performance of single fingerprint based beam-alignment and of line-of-sight (LOS) falls down precipitously with the increase of traffic density. This is because with the increase of traffic density, the probability of LOS blockage becomes high, hence resulting in low RSS. On the other hand, the single fingerprint based beam-alignment, which is designed for a given traffic density[9] and uses the same fingerprint for other traffic densities suffers from blockages, since the beam-pair suitable to one setting is unsuitable for another. Furthermore, the desired AoA-AoD pair which is suitable for that specific setting may be absent from the fingerprint constructed for another setting. Therefore, the performance is significantly affected. By contrast, the multiple fingerprint based design provides better performance; however, it can be seen that multiple fingerprint based adaptation without learning is unable to always maintain the target RSS. Instead it is hovering around it owing to the ever-changing channel statistics imposed by the changes in the environment. Hence, employing learning in our multiple fingerprint based design would intelligently adapt to the time-variant environment so that it always meets the target RSS, as shown in Fig. 11.

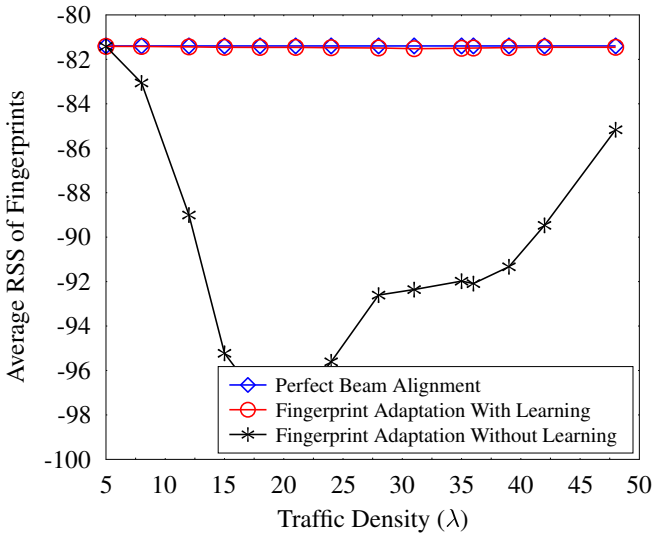

Fig. 12. Average RSS values over all the beam-pairs in the fingerprint observed at the user for $v < -0.7$.

Fig. 12 shows the average RSS values over all the beam-pairs in the selected fingerprint after adaptation versus the traffic density. More explicitly, it is a measure of the total average received power observed within a given fingerprint, which is the power observed after post-processing, if the transmit power is equally shared across the beam-pairs in the fingerprint. The rationale of choosing this metric is to study the impact of the average RSS power over all the beam-pairs when the transmit power in each beam is constant. It is evident from the figure that the fingerprint selected using learning performs similarly to perfect beam-alignment, where an exhaustive beam sweeping is carried out. The physical significance is that the receiver is able to capture the signal from all the directions predicted by our learning algorithm. In other words, the learning accurately predicted the fingerprint that is comprised of maximum possible number of beam-pairs for successful link-connection, which is also observed in the average RSS. On the other hand, the fingerprint selection dispensing with the learning is significantly affected, as seen in Fig. 12, due to poor selection of the fingerprint, i.e. when the fingerprint associated with the wrong beam-pairs is selected. To elaborate further, the fingerprint that is selected does not contain the beam-pairs for successful transmission, which means that the transmit power allotted to these beam-pairs suffer blockages or experience deep fading[10], hence resulting in low average RSS values at the user. It is important to emphasize that our proposed design achieves the performance of perfect beam-alignment at a significantly reduced search complexity.

Fig. 13 shows the probability distribution function (PDF) of the fingerprints against the traffic density. It can be seen in Fig. 13a that as the number of vehicles or as the traffic density increases, the PDF of fingerprint 1 starts falling gradually, while fingerprint 2 increases monotonically. Similarly, as the the traffic density increases further, the PDF of fingerprint 2 falls and the PDF of fingerprint 3 starts to increase. This implies that the set of beam-pairs in the fingerprint that provides a successful alignment starts to fall because of the increase in blockages caused by the increase in traffic density. Hence, the fingerprint which has the beam-pairs suitable for that environment is selected for a successful transmission. For example, when considering the traffic density range between 5-to-20, the PDF of fingerprint 1 falls because, whenever the set of beams in it is blocked due to the increased density of vehicles, it selects fingerprint 2 with the aid of the learning model developed during the training phase, since it provides alternate beam-pairs for link-connection. Fig. 13b shows the PDF of the fingerprints, when dispensing with learning. It can be noticed here that switching from one fingerprint to other fingerprint is different from that observed in Fig. 13a, as the switching is decided based solely on the look-up table, which may be outdated because of the time-varying nature of the channel.

Fig. 14 shows the average RSS observed in the beam-pairs chosen from the selected fingerprint at the receiver. It is important to note the difference between Fig. 14 and Fig. 12, where the latter is the average RSS observed in all the beam-pairs of the selected fingerprint. Fig. 14 depicts the RSS for two values of v, i.e. for different vehicular heights. In this investigation, we have set the target RSS to -82 dB. It can be seen that for both cases of v the learning aided design performs

[8]In LOS based beam-alignment, the beam is steered in the direction of the user, which is obtained from location, without account for blockages.

[9]In our simulation, we have designed the single fingerprint for a traffic density λ of 5.

[10]In this plot, since $v < -0.7$, the reduced RSS values should be attributed to only channel fading, as there is no attenuation due to vehicles. Hence the look-up table based fingerprint selection degrades the performance because of the channel imperfections as discussed in Sec. III-A.

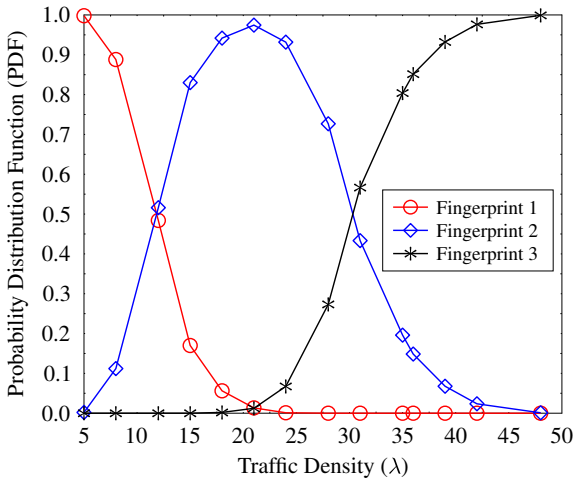

(a) Probability distribution function of fingerprints when learning is employed.

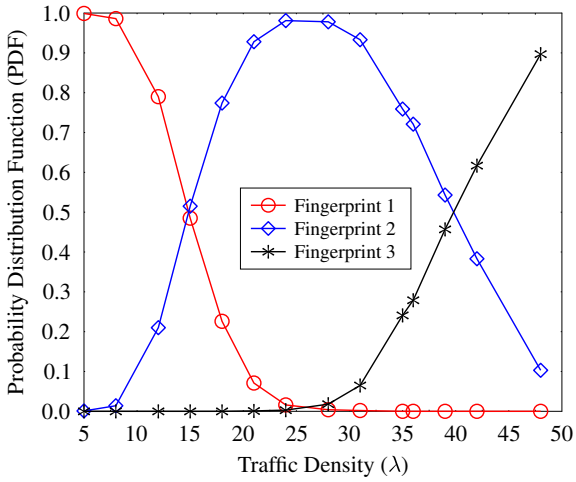

(b)

Fig. 13. Probability distribution function of fingerprints dispensing with learning.

about 1 dB higher than the target RSS. By contrast, the design relying on look-up table suffers significantly, especially in the traffic density regions between 10-15 and 30-40. This performance is akin to that of the conventional link-adaptation designs.

Fig. 15 shows the rate of our proposed design with learning and dispensing with learning. It can be seen from Fig. 15 that the rate of the design dispensing with learning is inferior to that of the learning-aided beam-alignment, while the design with learning provides the maximum rate of 2 bpcu regardless of the vehicular density. This is because the design without learning relies on the threshold values of the look-up table which suffers from blockages in the traffic density regions between 10-15 and 30-40.

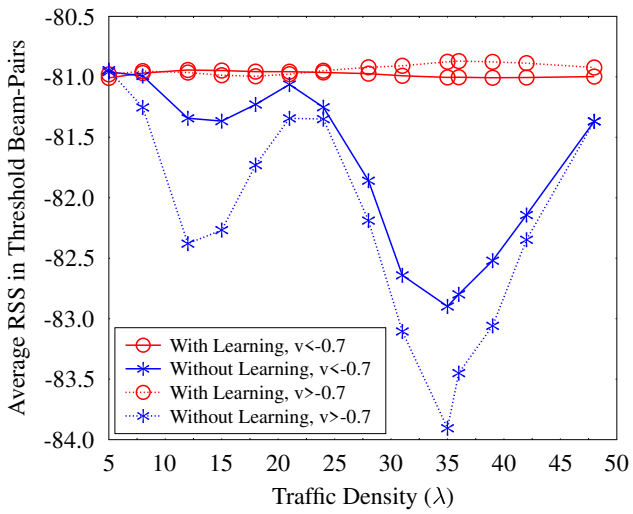

Fig. 14. Average RSS values observed at the receiver in the specifically selected beam-pairs which meet the target RSS.

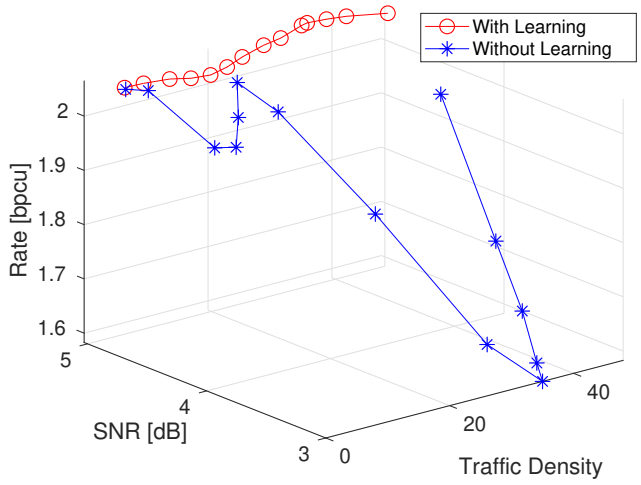

Fig. 15. Rate observed at the receiver in the selected beam-pairs.

V. Complexity

In this section, we discuss the complexity of the designs presented. The conceptually simple beam-sweeping technique, imposes substantial complexity during the beam-search. Let us consider a signal departing at an angle $\theta_d \in (0, 360^\circ)$ from the transmitter, which is being received at an angle $\theta_r \in (0, 360^\circ)$ by the receiver. Let us also assume that the half-power beamwidth (HPBW) of the signal ray is β. Then a beam-sweeping based beam-alignment has to perform an exhaustive search over $\left(\frac{360}{\beta}\right)^2$ beam-pair combinations. On the other hand, the fingerprint based beam-alignment imposes a much lower complexity, since the number of beam-pairs is significantly reduced. We note that the complexity of the proposed design predominantly arises in the learning stage, which is carried out in an offline fashion. In other words, the weights of Fig. 4b are designed prior to any communication

between the BS and the user, which then are stored in memory whose storage complexity[11] between two layers of the network is on the order of $\mathcal{O}(n_i n_j) + \mathcal{O}(n_j)$, where n_i and n_j are the number of neurons (or nodes) between the layers i and j, respectively. More particularly, the complexity in our design depends on the number of computations it has to perform while applying the weights in real time. To elaborate further, let us consider Fig. 4b, and for the sake of simplicity let us assume that there are $n_i = n_j = n$ neurons in each hidden layer, while the input vector $\mathbf{x}_i$ also has a dimension of n. Then the total number of computations, i.e. additions and multiplications, needed for h hidden layers is on the order of $\mathcal{O}(hn^2)$. Furthermore, it is important to emphasize that the complexity of any learning algorithm depends on the input dimensionality [29], [40] (the input vector $\mathbf{x}_i$ is referred as *feature set* in machine learning), which is however, only three-dimensional in our design.

VI. Conclusions

Given the ever-changing traffic density, we proposed a multi-fingerprint based database that adapts intelligently between different fingerprints with the aid of learning. Furthermore, as an extension to our proposed design, we presented an application to enhance the spectral efficiency as well as the performance by multi-functional beam transmission, where the beam-pairs that satisfy the required received signal strength participate in increasing the spectral efficiency. We demonstrated by our simulations that having a multiple fingerprint-based beam-alignment provides superior performance over the single fingerprint based beam-alignment. Furthermore, we showed that our learning-aided multiple fingerprint design provides better fidelity than that of the scheme employing multiple fingerprints but dispensing with learning. Additionally, our proposed learning-aided beam-alignment design performs similarly to that of beam-sweeping based beam-alignment where an exhaustive beam-search is carried out, at a reduced search complexity. More explicitly, our design is capable of maintaining the target RSS in dense vehicular environments, while both single fingerprint and line-of-sight (LOS) based beam-alignment suffer from blockages.

References

[1] I. A. Hemadeh, K. Satyanarayana, M. El-Hajjar, and L. Hanzo, "Millimeter-wave communications: Physical channel models, design considerations, antenna constructions, and link-budget," *IEEE Commun. Surveys Tuts.*, vol. 20, no. 2, pp. 870–913, Secondquarter 2018.

[2] K. Satyanarayana, M. El-Hajjar, P. Kuo, A. Mourad, and L. Hanzo, "Dual-function hybrid beamforming and transmit diversity aided millimeter wave architecture," *IEEE Trans. Veh. Technol.*, vol. 67, no. 3, pp. 2798–2803, March 2018.

[3] M. Boban, T. T. V. Vinhoza, M. Ferreira, J. Barros, and O. K. Tonguz, "Impact of vehicles as obstacles in vehicular ad hoc networks," *IEEE J. Sel. Areas Commun.*, vol. 29, no. 1, pp. 15–28, January 2011.

[4] V. Va, T. Shimizu, G. Bansal, and R. W. Heath, "Beam design for beam switching based millimeter wave vehicle-to-infrastructure communications," in *Proc. ICC*, May 2016, pp. 1–6.

[11] During the training phase of the neural network, a sufficient number of training samples are stored. In our simulations, we have used around 1000 training samples. Please note that the training samples may be discarded once the training weights have been designed, since only the training weights are needed during the testing phase.

[5] G. H. Mohimani, F. Ashtiani, A. Javanmard, and M. Hamdi, "Mobility modeling, spatial traffic distribution, and probability of connectivity for sparse and dense vehicular ad hoc networks," *IEEE Trans. Veh. Technol.*, vol. 58, no. 4, pp. 1998–2007, May 2009.

[6] M. J. Farooq, H. ElSawy, and M. Alouini, "A stochastic geometry model for multi-hop highway vehicular communication," *IEEE Trans. Wireless Commun.*, vol. 15, no. 3, pp. 2276–2291, March 2016.

[7] IEEE, "IEEE std 802.11ad-2012," pp. 1–628, 2012.

[8] T. Nitsche, C. Cordeiro, A. B. Flores, E. W. Knightly, E. Perahia, and J. C. Widmer, "IEEE 802.11ad: directional 60 GHz communication for multi-Gigabit-per-second Wi-Fi [invited paper]," *IEEE Commun. Mag.*, vol. 52, no. 12, pp. 132–141, December 2014.

[9] J. Wang, "Beam codebook based beamforming protocol for multi-Gbps millimeter-wave WPAN systems," *IEEE J. Sel. Areas Commun.*, vol. 27, no. 8, pp. 1390–1399, October 2009.

[10] S. Hur, T. Kim, D. J. Love, J. V. Krogmeier, T. A. Thomas, and A. Ghosh, "Millimeter wave beamforming for wireless backhaul and access in small cell networks," *IEEE Trans. Commun.*, vol. 61, no. 10, pp. 4391–4403, October 2013.

[11] J. Zhang, Y. Huang, Q. Shi, J. Wang, and L. Yang, "Codebook design for beam alignment in millimeter wave communication systems," *IEEE Trans. Commun.*, vol. 65, no. 11, pp. 4980–4995, Nov 2017.

[12] C. Liu, M. Li, S. V. Hanly, I. B. Collings, and P. Whiting, "Millimeter wave beam alignment: Large deviations analysis and design insights," *IEEE J. Sel. Areas Commun.*, vol. 35, no. 7, pp. 1619–1631, July 2017.

[13] B. Li, Z. Zhou, H. Zhang, and A. Nallanathan, "Efficient beamforming training for 60-GHz millimeter-wave communications: A novel numerical optimization framework," *IEEE Trans. Veh. Technol.*, vol. 63, no. 2, pp. 703–717, Feb 2014.

[14] T. Kadur, H. L. Chiang, and G. Fettweis, "Effective beam alignment algorithm for low cost millimeter wave communication," in *Proc. VTC (Fall)*, Sept 2016, pp. 1–5.

[15] T. Nitsche, A. B. Flores, E. W. Knightly, and J. Widmer, "Steering with eyes closed: Mm-wave beam steering without in-band measurement," in *in Proc. INFOCOM*, April 2015, pp. 2416–2424.

[16] V. Va, J. Choi, T. Shimizu, G. Bansal, and R. W. Heath, "Inverse multipath fingerprinting for millimeter wave V2I beam alignment," *IEEE Trans. Veh. Technol.*, vol. 67, no. 5, pp. 4042–4058, May 2018.

[17] A. Capone, I. Filippini, and V. Sciancalepore, "Context information for fast cell discovery in mm-wave 5G networks," in *in Proc. EuWC*, May 2015, pp. 1–6.

[18] A. Capone, I. Filippini, V. Sciancalepore, and D. Tremolada, "Obstacle avoidance cell discovery using mm-waves directive antennas in 5G networks," in *Proc. PIMRC*, Aug 2015, pp. 2349–2353.

[19] J. C. Aviles and A. Kouki, "Position-aided mm-wave beam training under NLOS conditions," *IEEE Access*, vol. 4, pp. 8703–8714, 2016.

[20] S. H. Fang, T. N. Lin, and K. C. Lee, "A novel algorithm for multipath fingerprinting in indoor WLAN environments," *IEEE Trans. Wireless Commun.*, vol. 7, no. 9, pp. 3579–3588, September 2008.

[21] K. Wu, J. Xiao, Y. Yi, D. Chen, X. Luo, and L. M. Ni, "CSI-based indoor localization," *IEEE Trans. Parallel Distrib. Syst.*, vol. 24, no. 7, pp. 1300–1309, July 2013.

[22] Z. Wei, Y. Zhao, X. Liu, and Z. Feng, "DoA-LF: A location fingerprint positioning algorithm with millimeter-wave," *IEEE Access*, vol. 5, pp. 22 678–22 688, 2017.

[23] X. Wang, L. Gao, and S. Mao, "CSI phase fingerprinting for indoor localization with a deep learning approach," *IEEE Internet of Things J.*, vol. 3, no. 6, pp. 1113–1123, Dec 2016.

[24] Z. E. Khatab, A. Hajihoseini, and S. A. Ghorashi, "A fingerprint method for indoor localization using autoencoder based deep extreme learning machine," *IEEE Sensors Lett.*, vol. 2, no. 1, pp. 1–4, March 2018.

[25] M. Giordani, A. Zanella, T. Higuchi, O. Altintas, and M. Zorzi, "Performance study of LTE and mmwave in vehicle-to-network communications," *CoRR*, vol. abs/1805.04271, 2018. [Online]. Available: http://arxiv.org/abs/1805.04271

[26] C. Jiang, H. Zhang, Y. Ren, Z. Han, K. Chen, and L. Hanzo, "Machine learning paradigms for next-generation wireless networks," *IEEE Wireless Commun.*, vol. 24, no. 2, pp. 98–105, April 2017.

[27] X. Wang, L. Gao, S. Mao, and S. Pandey, "CSI-based fingerprinting for indoor localization: A deep learning approach," *IEEE Trans. Veh. Technol.*, vol. 66, no. 1, pp. 763–776, Jan 2017.

[28] H. Chen, Y. Zhang, W. Li, X. Tao, and P. Zhang, "Confi: Convolutional neural networks based indoor Wi-Fi localization using channel state information," *IEEE Access*, vol. 5, pp. 18 066–18 074, 2017.

[29] C. M. Bishop, *Pattern Recognition and Machine Learning (Information Science and Statistics)*. Berlin, Heidelberg: Springer-Verlag, 2006.

[30] J. Wang, C. Jiang, H. Zhang, Y. Ren, K.-C. Chen, and L. Hanzo, "Thirty years of machine learning:the road to pareto-optimal next-generation wireless networks," 2019. [Online]. Available: http://arxiv.org/abs/1902.01946
[31] C. Feng, W. S. A. Au, S. Valaee, and Z. Tan, "Received-signal-strength-based indoor positioning using compressive sensing," *IEEE Trans. Mobile Comput.*, vol. 11, no. 12, pp. 1983–1993, Dec 2012.
[32] S. Han, C. I, Z. Xu, and C. Rowell, "Large-scale antenna systems with hybrid analog and digital beamforming for millimeter wave 5G," *IEEE Commun. Mag.*, vol. 53, no. 1, pp. 186–194, January 2015.
[33] X. Zhang, A. F. Molisch, and S.-Y. Kung, "Variable-phase-shift-based RF-baseband codesign for MIMO antenna selection," *IEEE Trans. Signal Process.*, vol. 53, no. 11, pp. 4091–4103, 2005.
[34] K. Satyanarayana, M. El-Hajjar, P. Kuo, A. Mourad, and L. Hanzo, "Millimeter wave hybrid beamforming with DFT-MUB aided precoder codebook design," in *Proc. VTC*, Sep. 2017, pp. 1–5.
[35] LTE; physical layer — measurements. [Online]. Available: https://www.etsi.org/deliver/etsi
[36] ITU-R. Propagation by diffraction. [Online]. Available: https://www.itu.int/rec/R-REC-P.526-11-200910-S/en
[37] T. M. Cover and J. A. Thomas, *Elements of Information Theory (Wiley Series in Telecommunications and Signal Processing)*. New York, NY, USA: Wiley-Interscience, 2006.
[38] X. Gao, L. Dai, C. Yuen, and Z. Wang, "Turbo-like beamforming based on tabu search algorithm for millimeter-wave massive MIMO systems," *IEEE Trans. Veh. Technol.*, vol. 65, no. 7, pp. 5731–5737, July 2016.
[39] Automotive technical data and specifications. [Online]. Available: http://www.carfolio.com/
[40] R. O. Duda, P. E. Hart, and D. G. Stork, *Pattern Classification (2Nd Edition)*. New York, NY, USA: Wiley-Interscience, 2000.